BEHAVIOUR OF AXIALLY LOADED CONCRETE COLUMNS SUBJECTED TO TRANSVERSE IMPACT LOADS

Thilakarathna H.M.I., School of Urban Development, Queensland University of Technology, Australia
Thambiratnam D., School of Urban Development, Queensland University of Technology, Australia
Dhanasekar M. , School of Urban Development, Queensland University of Technology, Australia
Perera N.J., Robert Bird Groups & School of Urban Development, Queensland University of Technology, Australia

Abstract

Increased industrialisation has brought to the forefront the susceptibility of concrete columns in both buildings and bridges to vehicle impacts. Accurate vulnerability assessments are crucial in the design process due to the possible catastrophic nature of the failures that can occur. This paper reports on research undertaken to investigate the vulnerability of columns in low to medium rise buildings, designed according to the Australian standards. Numerical simulation techniques were used and validation was done by using experimental results published in the literature. The material model formulation used for validation is scrutinised and numerical tests are preformed to examine its ability to simulate the impact conditions.

Axially loaded columns made out of grade 40 to 50 concrete with two different steel ratios are considered in the analyses. It is found that typical columns in five storey buildings, having a high slenderness ratio of 13.33, are highly vulnerable to medium velocity car impacts [1]. The investigations are continued with different combinations of parameters to identify the means to mitigate damage. It is observed that the design option with low amount of steel significantly improves impact capacity while a higher grade of concrete considerably increases the vulnerability of the impact, contrary to what would be expected. However, further improvements can be made when smaller slenderness ratios are selected. In particular, influences of time of impact and iso-damage conditions are investigated in detail. It has also been found that vehicle impacts can be categorised next to the quasi-static loading region in typical force-impulse diagrams. This will allow numerical methods to be implemented to quantify the impact damages.

Key words: Dynamic analysis, Numerical simulations, Lateral impact, Structural columns

1.0 *Introduction.*

Exposed columns in underground car parks and the frontal columns in buildings located along the roads are highly vulnerable to impact loads due to moving vehicles. Progressive failure of supporting structure, as a result of the impact worsens the consequences and may require proper analysis techniques which can be used for routine column design. However, the behaviour of concrete under extreme loading conditions is not well understood [2]. Higher modes of vibrations, strain rate effects, confinement effects, as well as the vehicle specific parameters further complicate the problem as far as the analysis process is concerned. On the other hand, simplified methods used in the past have several inherent limitations and therefore may or may not be robust.

Hence, this paper briefly overviews the constitutive material model and Improvements are introduced to simulate the tensile and shear characteristic under typical impact. The numerical simulation of a column is validated in the next stage by using the experimental data from an impacted column. Typical impact pulses generated from a car to rigid barrier impact were used in the process of impact reconstruction. Parameter sensitivity of the calibrated columns is investigated in the following phase, and the potential of the development of the practical design guidelines based on comprehensive parametric investigations are also highlighted.

2.0 Validation of the finite element model

2.1 Material model

Impact loads may generate tri-axial state of stress in concrete columns. For instance, from a material point of view, spalling occurs at the contact interface as a result of tri-axial extension stress conditions. Subsequent impacts on the column may generate tri-axial compression stress conditions in the core concrete. In the meantime, uni-axial tensile stresses will be generated at the opposite face by scabbing the concrete as a result of wave reflection at the boundaries. Therefore, a material model that can replicate the results of tri-axial extension tests, tri-axial compression tests, and uni-axial tensile tests must be used in the impact simulation process. Each of these tests will represent different damage modes. However, the possibility of combined mode of failures can not negligible.

The LS-DYNA material library has several material models that can be used to simulate the impact behaviour of concrete [3]. The material model Concrete_Damage_REL3 is used in this investigation to simulate the concrete. The advantage is that unconfined compressive strength and density of concrete are the only parameters that are required in the calibration process. However, if the response significantly differs from the observed behaviour of concrete then improvement can be introduced via additional model parameter calibration [4]. In addition, the code utilizes the unconfined compressive and tensile tests paths to implement the rate enhancement effects. This method will enable enhancement of the strength equally along any stress path and hence the different failure stress states such as uniaxial, biaxial and triaxial tension, and uniaxial and biaxial compression all remain unaffected. Moreover, this model uses three shear failure surfaces; namely an initial yield surface, a maximum failure surface and a residual surface with consideration of all the three stress invariants (I_1, J_2 and J_3). Therefore it can effectively simulate the tri-axial state of stress conditions.

2.2 Determination of damage evolution parameters b_2 and b_3

As the softening part of the unconfined uni-axial tension stress-strain curve is governed by the values of two parameters b_2 and b_3, these parameters have to be adjusted to minimise the differences between the numerical and the experiment results [5]. For example, the softening behaviour becomes mesh-dependent if it is not governed by a localization limiter or characteristic length. Thus, the mesh dependency of the fracture energy has to be corrected by changing the parameters accounted for the tensile softening of the material. The mesh dependency can be eliminated by selecting 'h', ie. the size of the finite element so that the ratio G_f/h equal to the area under the stress-strain curve for the uniaxial unconfined tensile test. Where G_f is the fracture energy of the concrete. This procedure will eliminate the mesh size dependency on the fracture toughness. However effects of the mesh topology on crack direction still persists in the numerical simulation.

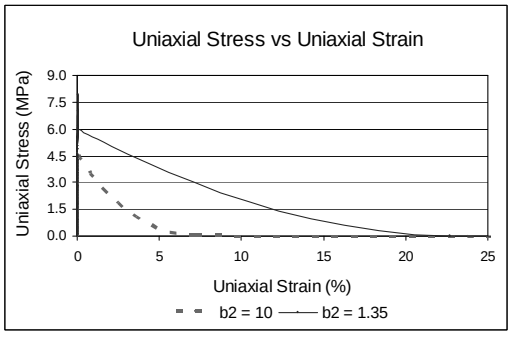

Figure 1: Single element under uni-axial tensile test

Figure 1 shows the stress-strain response of a single element (1x1x1mm) subjected to uni-axial tension test. According to the CPF-FIP model code, the fracture energy of Grade 50 concrete should be around 105 N/m to 130 N/m [6]. Hence, the default value of b_2 (b_2=1.35) will overestimate the fracture toughness of Grade 50 concrete. Therefore, the value of the b_2 is adjusted until the area under the stress-strain curve becomes 120 N/m. Similarly, parameter b_3 has to be found by using a hydrostatic tri-axial tensile test. However, the default value of b_3 seems to be acceptable. The effects of these parameters are more obvious when the tensile or shear failures are predominant.

2.3 Experimental setup and the validation of the numerical model

Experimental results of the Feyarabend [7] column tests were used in the validation process. The column was tested in a horizontal position as shown in Figure 2. Fixed support conditions was achieved by stationary steel sections fixed at the ground and the other end was hinged and free to slide parallel to the longitudinal axis of the column while being restrained by a 20t mass. The mass

can slide over horizontal low friction rails. The axial load is applied by using a prestressing wires located on either sides of the column and impact load was generated by dropping the 1.14t mass on to the column at mid span. Under the mid span impact the column has reached near failure conditions. The properties of the test specimen are tabulated in Table 1. More descriptive details of the development of the numerical model and validation can be found from Thilakarathna et al. [1].

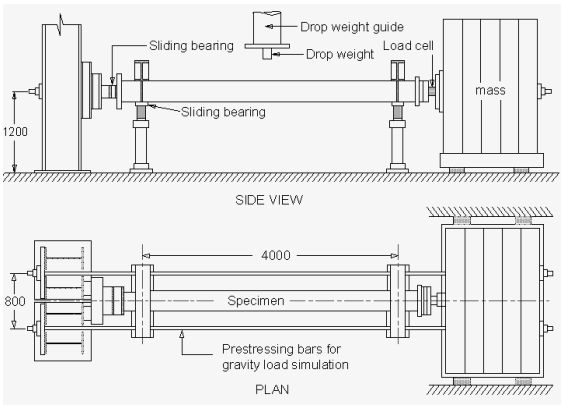

Figure 2: The test set-up by Feyerabend [7]

Test	SB1
Cross-section (mm)	300x300
Span (m)	4.0
Cube strength, f_{cu} (MPa)	44
Yield stress, f_y (MPa)	482
Main bars, A_s	4ϕ18
Shear reinforcement, A_{vs}	12ϕ@150
Restraining mass (t)	20
Initial axial load (kN)	-245
Striker mass (t)	1.14
Impact velocity (m/s)	1.5/3.0
Velocity at which f_y was reached (m/s)	±1.5

Table 1: Characteristics of the Feyerabend's test specimens [7]

2.4 Numerical results

Some of the essential results of the numerical simulation are summarised here in brief. According to the Figure 3, the resultant maximum deflection, residual displacement and duration of the impact are well reflected by the numerical simulation. Therefore the inertia stiffness of the impacting bodies, boundary conditions and effects of confinement are accurately simulated by the numerical model. However, failure strain was not defined to simulate the cracking and slightly crushing behaviour of the concrete during the impact. This could be one of the reasons for the oscillatory behaviour of the numerical model at its residual stage. As far as the contact force history is concerned (Figure 4), it can be seen that the differences between those two graphs are insignificant and the fluctuations are almost identical. In fact, the exact simulation of the peak contact force is an evidence of the accurate representation of the stiffness and boundary conditions as it would mainly depend on the inertia characteristics of the column for given boundary conditions.

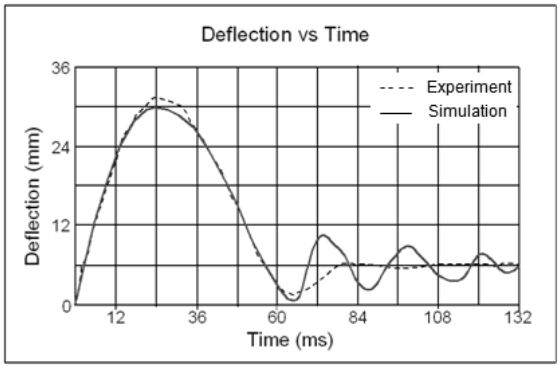

Figure : 3 Comparison of the resultant deflection

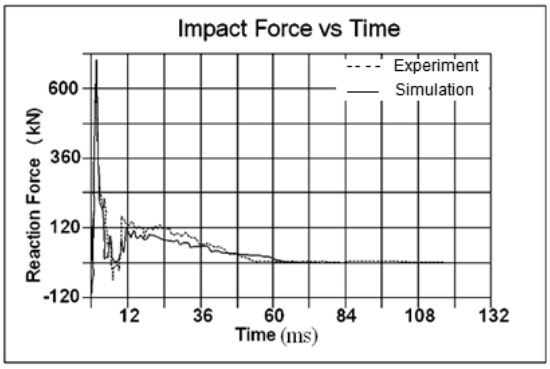

Figure : 4 Comparison of the resultant impact force

3. Impact reconstruction by using crash test data

Due to the complexity of generating realistic numerical models of vehicles for impact reconstructions, the force time histories generated from the full scale crash tests were used in the numerical simulation process. However, the crash response depends on the mode of impact, rate sensitivity of the vehicle, dynamic crush, restitution, collision partner and vehicle specific parameters [8]. Therefore the characteristics of the unknown pulse were determined by using full-scale car impact test with rigid barriers to reduce variations, which yield conservative vulnerability assessments [1].

Numerous models have been proposed to simulate the impact pulse with varying success. Sine, haversine, triangular and square formats are the standard formats that have been widely used to represent the frontal barrier impact [8]. To investigate the efficiency of the various curves to simulate the collision pulses, force histories generated from several full scale frontal collision scenarios were studied by using MATLAB program. Based on this, several force histories derived by using accelerometer data presented in SAE [9] are compared. Figure 6 shows the comparisons of the Force -Time history of the Honda Accord, Ford Taurus & Renault Fuego for typical head on collisions. Durations of the impacts were 100ms and triangular pulse shape is best fitted with the force history

diagrams. This pulse shape has already been identified as a useful collision pulse model to simulate the frontal impact conditions [10]. At the next stage the duration will be varied to account for stiffness variations. Since the product of the mass and velocity of the impacting vehicle is equal to the area under the force history diagram [1], peak force can be adjusted to account for the various impact speeds. However, it is worth to note that the there is a noticeable loading shape influence on the force impulse diagram in the dynamic region where both the peak load and impulse play a major role in dertermine the structural response [11].

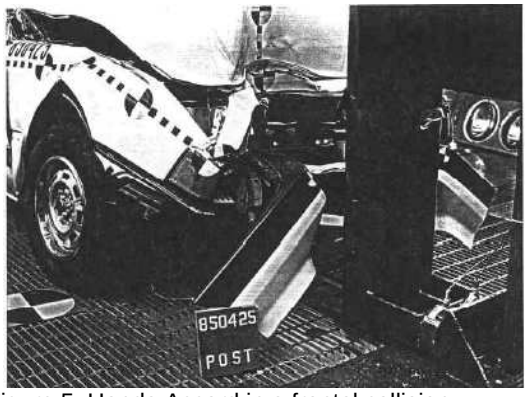

Figure 5: Honda Accord in a frontal collision at a speed of 48.3km/h [9]

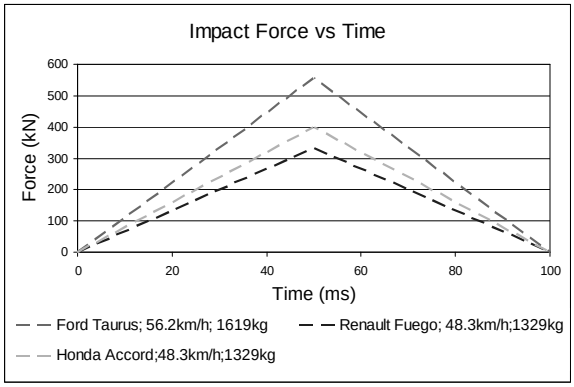

Figure 6: Force Time histories of full scale crash tests

4. Impact behavior of axially loaded column

Impact capacity of typical braced columns of five to twenty storied buildings made out of Grade 40 to 50 concrete was investigated by using comprehensive numerical simulations. Considered columns are supporting 6m spaning slabs in each direction which carries 3kN/m^2 live load identical to the design load capacity of an office building, classrooms or lecture theatres at each floor level [12]. Vulnerability of a ground floor column was assessed for a typical frontal collision of light weight vehicles such as cars or vans. The structural design is carried out by assuming general design prospective according to AS3600 standards [12]. However for comparison purposes the axial stresses on the columns is maintained approximately constant rather than the axial load on the columns. This leads to smooth graphs at the later stage. In addition, two alternative design options with two different steel ratios were considered and Figure 7 represents the cross sections of the selected columns for different storey height.

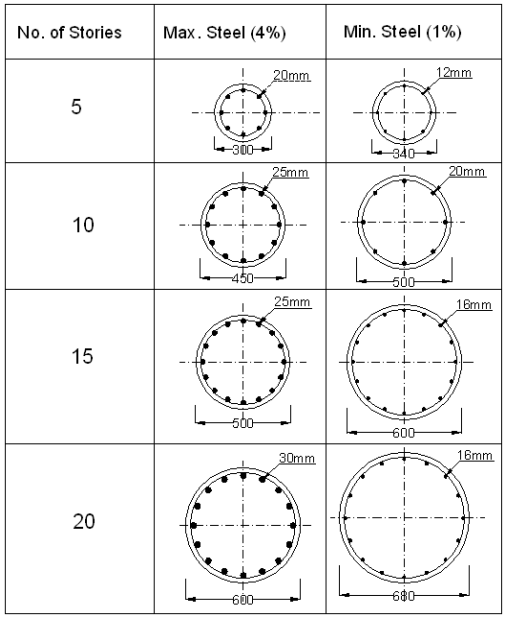

Figure 7: Cross sectional area of the circular concrete columns

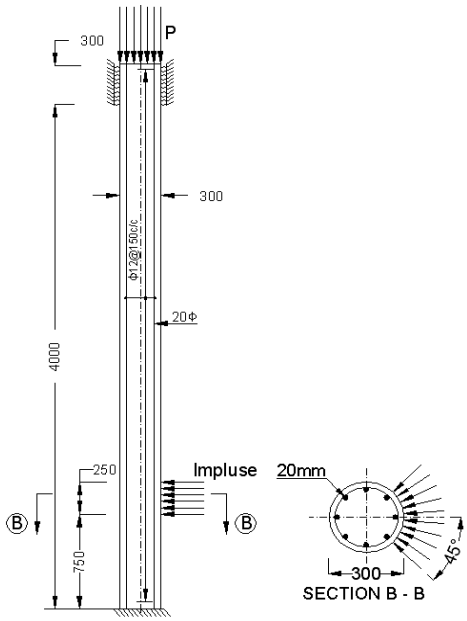

Figure 8: Support conditions and external loads applications

4.1 **Vehicle- column interaction**

The area of contact has some correlation with the mode of failure and the dissipation of kinetic energy through structural deformation. Therefore, the vulnerability will depend on the distribution of the

pressure over the contact interface. EN 1991(2006) suggested that the contact area should be 0.25m height for car impact [13]. However, there is no guidance on the lateral distribution of the pressure across the section, particularly for circular columns (Figure 8). Figure 10 shows a rigid pole used to carry out several full scale impact tests on cars [8]. It is evident that the effective contact area is around 0.25% of the perimeter if the frictional effects are neglected. Therefore, uniform and perpendicular pressure distribution is assumed across the 0.25% of the perimeter and the resultant lateral pressure distribution given in Figure 9.

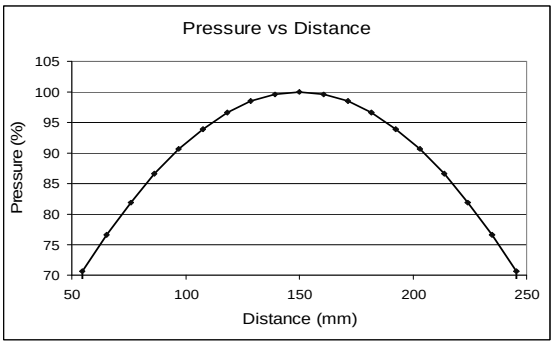

Figure 9: Lateral pressure distribution across the diameter of the 300mm column

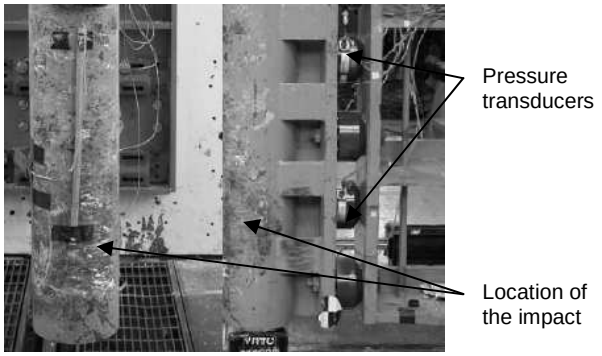

Figure 10: Front and side views of an impacted column

4.2 Possible damage modes

In fact, failure due to vehicle impact is varied from the usual flexural type of failures during a mid span impact. Therefore, a conventional hypothesis based on the energy absorption capacity of the column may not be applicable as the energy absorption characteristics mainly depend on the flexural deformation of the column. Since the column not subjected to flexural deformations, a small portion close to the impacted region undergoes highly localised stress and absorbs an excessive amount of energy before the remaining portion of the column. This localised stress will exceed the yield stress of the concrete and hence may fail abruptly during the impact. This will considerably reduce the effective area of the column and the resultant eccentric axial load will finally diminish the axial load carrying capacity of the column. Under this circumstance, the column will fail due to shear failure initially and subsequently by flexural failure to collapse. The observed failure modes can be categorised as shear or shear flexural type of failures depending on the test variables. However, failures due to higher modes of vibration are not detected for the circular columns.

5. Parametric studies

Based on the above reasons, it is expected that the parameters that govern the flexural shear type of failures under quasi-static loading condition can be effectively used to quantify the damage under impact conditions. A comparative analysis revealed that the flexural-shear failure conditions of the columns are well predicted by the AASHTO equations for bridge piers, ATC/MCTTER equations, equations by Ascheim and Moehle and equations by priestly et al. [14]. In these equations, the total shear capacity of a column was calculated by adding together the contribution of the steel and concrete. It can be seen that the most of the parameters are common and therefore the effect of these terms are further investigated in the parametric study.

5.1 Effects of the diameter of the column, concrete grade and steel ratio

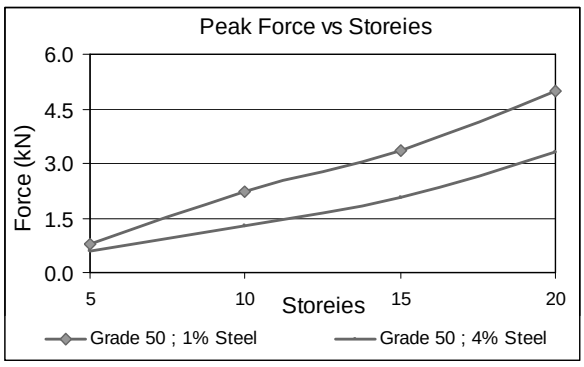

Figure 11: Effects of the diameter of the column

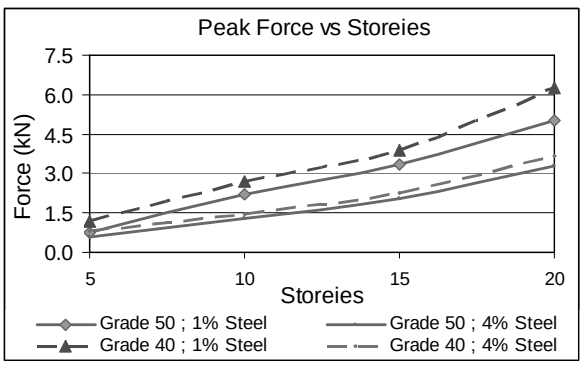

Figure 12: Effects of the concrete grade

Impact capacities of the columns at each storey level and the capacity variation with the grade of concrete are shown in figure 11 and 12 along with the two steel ratios. Selected column diameters at each storey height are given in Figure 7. The axial stress on the columns was maintaned almost constant for a particular grade of concrete. The highest gain of the impact capacity is obtained with columns having low amount of steel with larger diameters. Therefore, at the design stage, impact capacity of the columns can be increased by 20% by selecting the alternative design method with the low amount of steel (Figure 11). In other words, the diameter of the column or the shear stiffness of the column will be one of the main parameters that controls its response. On the other hand, according to Figure 12 columns made out of grade 40 concrete can withstand higher impact loads than its counterpart. Bischoff and Perry [15] also observed that the energy absorption capacity of the lower grade of concrete are higher compared to that of the higher grade of concrete. Thus, an equivalent column of lower grade concrete with low amount of steel will offer maximum protection against car impact conditions. Incidentally, the contribution of the steel to mitigate the damage due to impact is less pronounced as the reinforcement does not have enough time to react and hence to develop its full strength against impact by reaching the nonlinear range. However, the impact capacity of the column is depends on the distribution of the longitudinal steel across the perimeter of the section.

5.2 Effects of the slenderness ratio

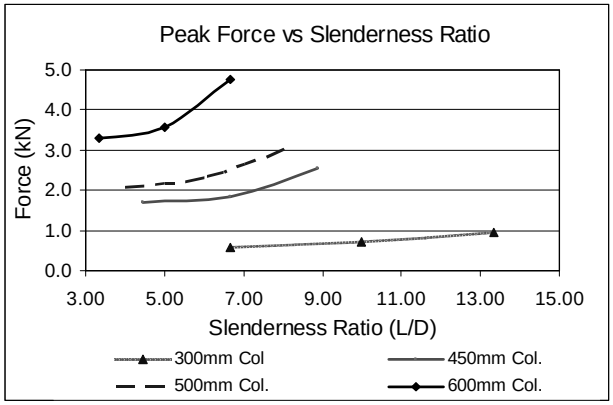

Figure 13: Effect of the slenderness ratio

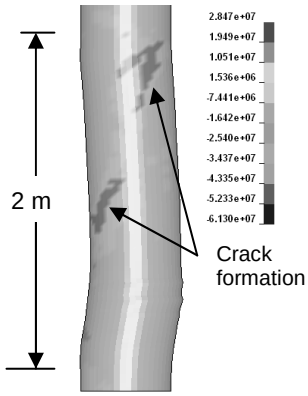

Figure 14: 500mm column with 4% steel

The effectiveness of slenderness ratio is investigated in Figure 13. As the slenderness ratio decreases, the failure plane will change its inclination. Concequently, the diagonal cracks are formed between the support and the point where maximum moment is reached followed by initial tension cracks (Figure 14). This change will increase the fracture energy dissipation through the cracked surface while increasing the number of effective links in preventing the crack propagation. Thus, noticeable 50% improvement in the critical peak force can be achieved on average. Apart from that, improvements are increased with the columns having larger diameters (Figure 13). As far as the effect of boundary conditions are concerned, there is no significant contribution from the supporting conditions to resist the impact force. However, slight increments can be seen when the slenderness ratio is higher and the difference will be decreased with the enhancement of the diameter.

5.3 Energy absorption due to the impact

Energy absorption will primarily depend on the failure mode which in turn governed by the specific parameters such as slenderness ratio, steel ratio, concrete grade, contact interface parameters etc. However, energy consumption for plasticity and nonlinear deformation are compatively low under impact conditions. Due to the localised damages and the microcracks, most of the energy dessipation will takes place closer to the contact interface. Therefore, fracture tougness of the concrete gained the highest consideration among the parameters that influence the energy dissipation of concrete rather that the tensile strength. Consequently, the energy absorped by the concrete is comparatively low and the most of the internal energy is stored as strain energy in the longitudinal steel.

5.4 *Effects of the duration of the impact*

The Figure 15 examines the impact characteristics of a 600mm diameter column with 4% steel. The column was subjected to constant impulses (ie: product of mass and velocity) with different durations and these impulses replicate the cars with constant mass with different frontal stiffness. Numerical results revealed that the column was failed under 50ms impact while the column subjected to 150ms impact remains unaffected. This observation confirmed the importance of the frontal stiffness

characteristics of the vehicle that govern the impact behaviour of columns. At the next stage, the peak forces of the triangular pulses are adjusted until the iso-damage or equivalent damage conditions are achieved (Figure 16). This has proved that the column is highly sensitive to the amplitude of the impact and not to the associated impulse. Thus, the vehicle impact generated forces theoretically closer to the quasi-static loading category where the response becomes insensitive to impulse [3].

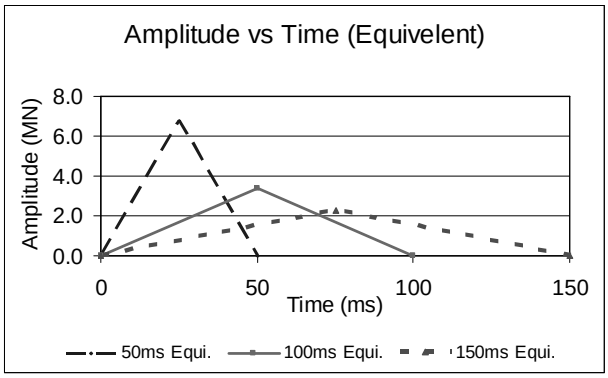

Figure 15: Equivalent impulse diagrams

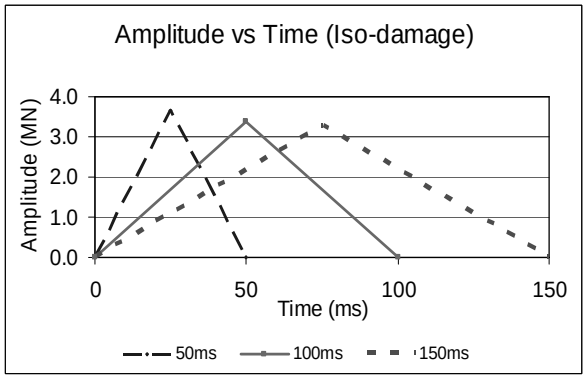

Figure 16: Iso-damade pulses for 600mm column

In addition, according to the Krauthammer et al. [16] if the load function follows the same pattern as the resistance function, such a scenario can be included in-between the dynamic and quasi-static regions (Figure 17). This observation also leads to the conclusion that the strain rate effects are less pronounce in the impact analysis. In general, the equivelent impulses must lead to the identical damage conditions as it represents the product of the mass and velocity of the impacted vehicle. However, the impact damages are not sensitive to the impulses and hence this rule is violated in the quasi-static region (Figure 16).

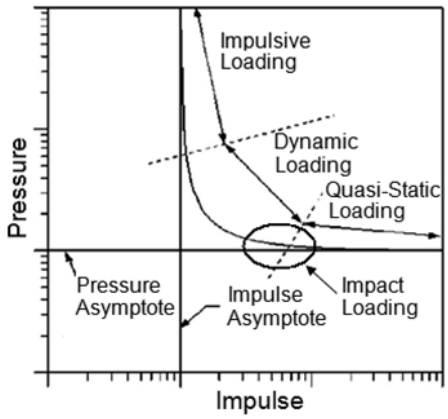

Figure 17: A typical Pressure impulse curve

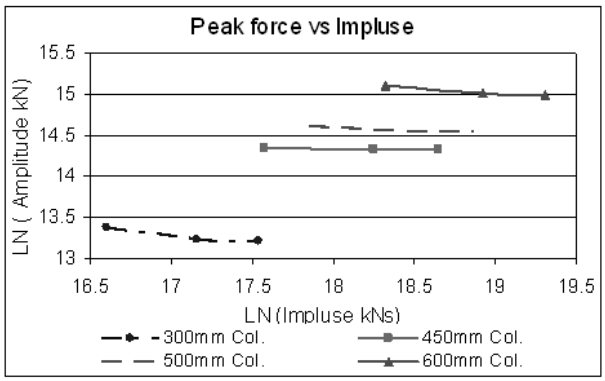

Figure 18: Iso-damage contours for impact

By considering all these factors, it is suggested that the vehicle impacts belong to a specific domain in the force impulse diagram. To investigate this hypothesis, force and the relative impulses that lead to the iso-damage conditions are plotted in a log scale for different column sizes (Figure 18). In fact, the curve reasonably agrees with the typical shape of the Force-Impulse diagram which is commonly adopted to predict the structural damage under blast loading conditions (Figure 17). Hence, the impact behaviour (in terms of *P, I*) can be expressed by the following mathematical expression which is valid between the dynamic and the quasi static regions.

$$(P - P_o)(I - I_o) = A\left(P_o/2 + I_o/2\right)^B \qquad \text{Eq: 1}$$

In the above equation, $P_o$and I_o represent a known force and impulse pair located on the iso-damage curve, *A* and *B* are constants to be determined based on the shape of the iso-damage contours. Similar expressions based on descending pressure pulses were used to describe the structural behaviour of columns under blast loading conditions [3]. However a unique set of equations will be required to determine the behaviour of columns under impact loading conditions where triangular pulses were applied over a limited area on the column to reconstruct the impact.

6. Conclusions

This paper treated the vulnerabilty of coulumns in medium rise buildings under vehicular impacts.The parameters invetigated are the concrete grade, steel ratio, impact duration, vehicle speed and support conditions. The main findings are listed below:

- A material model that can replicate tri-axial state of stress must be used in the impact simulation process. LS_DYNA material model Mat_Concrete_Damage_REL3 fulfils the requirement, but some modifications to the constitutive model may be needed under tensile or shear failures.
- Triangular impact pulses can be effectively used to simulate the frontal impact conditions and the average duration can be taken as 100ms. However the influence of the shape of the loading pulse on impact behaviour needs further investigation. If effects of friction are neglected, the effective contact area can be taken as around 0.25% of the perimeter of the column.
- Vehicle induced damages should be treated differently from the damages due to the mid span impact. The initial damage of the column is due to shear failure, but subsequently the column fails under flexural failure conditions. Consequently, stain rate does not have much effect.
- The vulnerability of axially loaded column under car impacts can be reduced by reducing the column aspect ratio, reducing the concrete grade and by choosing the design option with low amount of steel. Thus an equivalent column of lower grade concrete with low amount of steel and low aspect ratio will offer the maximum protection against impact loads.
- The impacts of columns treated herein are theoretically close to the quasi-static loading region where the response becomes insensitive to impulse but more sensitive to the peak force. This will support the argument that the second order strain rate effects can be negligible and emphasised the importance of the stiffness characteristics of the impacted vehicle. However the usual relationship between the mass and the velocity of the impacted vehicle to the area of the force history diagram will violate in this region.
- Iso-damage curves of the impacted columns will follow the shape of the conventional pressure impulse diagrams under blast loading conditions. However seperate set of equations will be required to quantify the impact damage as the pulse characteristics and area of contact different from those under blast loading.

7. References

[1] Thilakarathna, H.M.I., et al., *Vulnerability of Axially Loaded Columns Subjected to Transverse Impact Loads*, The second infrastructure theme postgraduate conference, 2009. 1(2): p. 22-35.

[2] Weerheijm, J. and J.C.A.M. Van Doormaal, *Tensile failure of concrete at high loading rates: New test data on strength and fracture energy from instrumented spalling tests*, International Journal of Impact Engineering, 2007. 34(3): p. 609-626.

[3] Shi, Y., H. Hao, and Z.X. Li, *Numerical derivation of pressure-impulse diagrams for prediction of RC column damage to blast loads,* International Journal of Impact Engineering, 2008. 35(11): p. 1213-1227.

[4] Schwer, E.L. and L.J. Malvar, Simplified concrete modelling with Mat_Concrete_Damage_ REL3. JRI LS_DYNA user week, 2005.

[5] Malvar, L.J., et al., *A plasticity concrete material model for DYNA3D*, International Journal of Impact Engineering, 1997. 19(9-10): p. 847-873.

[6] *CEB-FIP, CEB-FIP Model Code 1990*, Redwood Books, Trowbridge, Wiltshire, UK, 1990.

[7] Louw, M.J., G. Maritz, and M.J. Loedolff, *The Behaviour of RC Columns under Impact Loading*, The Civil Engineer in Sougth Africa, 1992: p. 371-378.

[8] Varat, M.S. and S.E. Husher, *Crash Pulse Modeling for Vehicle Safety Research*, 18th ESV Paper, 2000.

[9] http://www-nrd.nhtsa.dot.gov/database/nrd-11/veh_db.html**.**

[10] Breed, D.S., V. Castelli, and W.T. Sanders, A New Automobile Crash Sensor Tester. SAE Technical Paper 910655, 1991. Society of automotive engineers, Warrendale, PA.

[11] Li, Q.M. and H. Meng, *Pulse loading shape effects on pressure-impulse diagram of an elastic-plastic, single-degree-of-freedom structural model*, International Journal of Mechanical Sciences, 2002, p.1985-1998.

[12] *AS 3600, Concrete structures*, 2004: p. 185.

[13] *EN 1991-1-7:2006, Eurocode 1 - Actions on structures - Part 1-7*: General Actions & Accidental actions. Irish standards, 2006.

[14] Lee, J.-H., Seong-Hyun Ko, and J.-H. Choi, *Shear Strength and Capacity Protection of RC Bridge Column*, 2003.

[15] Bischoff, P.H. and S.H. Perry, *compressive behaviour of concrete at high strain rates*, Material and Structures, 1991. 24: p. 425-450.

[16] Krauthammer, T., et al., *Pressure-impulse diagrams for the behaviour assessment of structural components*, International Journal of Impact Engineering, Twenty-fifth Anniversary Celebratory Issue Honouring Professor Norman J designed according to the Australian standards ones on his 70th Birthday, 2008. 35(8): p. 771-783.